Direct experimental observation of different diffusive transport regimes in semiconductor nanostructures

M. Achermann,* B. A. Nechay, F. Morier-Genoud, A. Schertel,† U. Siegner, and U. Keller
Swiss Federal Institute of Technology Zurich, Institute of Quantum Electronics, ETH Honggerberg HPT, CH-8093 Zurich, Switzerland
(Received 20 January 1999)

A near-field pump-probe system with nanometer-scale spatial and femtosecond temporal resolution allows us to measure complex spatiotemporal carrier diffusion dynamics in semiconductor nanostructures. Single GaAs/Al$_x$Ga$_{1-x}$As quantum wells are patterned by nanometer-scale focused ion-beam (FIB) implantation, which introduces local carrier trapping. The resulting carrier density gradients cause diffusion, which is directly observed by measuring carrier density variations in both time and space. A comprehensive experimental study allows us to identify different diffusion regimes. We find an initial diffusion regime, characterized by nonsinusoidal carrier profiles and spatially dependent temporal diffusion decay. In a long-time regime, the carrier profile is quasisinusoidal and only weakly position-dependent temporal diffusion decay is observed. [S0163-1829(99)02827-1]

The temporal evolution of optically excited carrier densities in semiconductor nanostructures can be strongly affected by real-space carrier transport.[1] Such transport effects are particularly important in nanostructures due to their inherent lateral inhomogeneity. For example, potential gradients in quantum wires lead to drift.[2] Also, spatially varying optical properties can give rise to gradients in the carrier density, which cause diffusive transport.[3] In fact, the occurrence of carrier transport in nanostructures has been observed in a variety of experiments. These include spatially resolved, time-integrated experiments,[1,4–7] spatially resolved experiments with limited, 260 ps, time resolution,[2] and time resolved but spatially averaged experiments.[8] However, the direct observation of the detailed features of spatiotemporal transport dynamics in nanometer-scale structures requires both high spatial and high temporal resolution since the short length scales imply fast transport. Recently, femtosecond near-field scanning optical microscopes (NSOM) have been developed which provide femtosecond time and nanometer-scale spatial resolution.[3,9–12] The observation of carrier transport dynamics with these instruments has been reported in Refs. 3 and 11. However, the detailed features of diffusive transport were not explored.

In this paper, we experimentally demonstrate that diffusive carrier transport in semiconductor nanostructures results in complex spatiotemporal carrier dynamics on the picosecond time and the nanometer length scale. These experiments have been made possible by a recently developed femtosecond NSOM with 150-nm spatial and 250-fs temporal resolution and high sensitivity.[12] We have used nanostructured samples in which carrier drift can be neglected, facilitating the observation of the detailed features of carrier diffusion. Different diffusion regimes are identified. In an initial regime, we directly observe *nonsinusoidal* carrier density profiles in which the temporal diffusion decay depends on the spatial position. On longer time scales, a quasisinusoidal spatial carrier profile forms, in which the temporal diffusion decay is only weakly dependent on position, characteristic for the long-time diffusion regime. The femtosecond NSOM allows us to directly measure the shape of nanometer-scale

spatial carrier profiles at different times.

Semiconductor nanostructures have been obtained by nanometer-scale lateral patterning of an undoped 80-Å GaAs/Al$_{0.3}$Ga$_{0.7}$As single quantum well with focused ion-beam (FIB) implantation of 50-keV Ga ions. The implantation energy was chosen to create damage in the GaAs quantum well, according to transport of ions in matter (TRIM) simulations.[13] The local ion implantation results in defect formation. These defects give rise to carrier trapping with picosecond or sub-ps time constants, which decrease with increasing ion dose.[14,15] Besides carrier trapping, ion implantation causes a decrease of the optical nonlinearity of exciton[16] and continuum[15] transitions. Sample *A* is patterned with 100-nm implanted stripes with 2000-nm spaces at a dose 8×10^{11} cm^{-2}, sample *B* with 200-nm implanted stripes with 400-nm spaces at a dose 3×10^{12} cm^{-2}. For FIB implantation, the spatial defect profile has well-defined edges since TRIM simulations[13] show that the defects spread only 20 nm beyond the nominal width of the implanted stripes. To prepare the samples for the NSOM experiments, the GaAs substrate was removed by wet etching.

Carrier dynamics in these nanostructures have been measured by near-field pump-probe experiments in which carriers are uniformly excited over a 5–10-μm diameter area. The pump-induced transmission changes are detected in the optical near-field with a probe pulse, which propagates through an NSOM fiber and the sample. A detailed description of the femtosecond NSOM can be found in Ref. 12. All experiments have been carried out at room temperature with 15-meV-wide pump and probe spectra centered at the lowest heavy-hole exciton resonance of the quantum well at 1.475 eV. The pump fluence is 4 μJ/cm^2, corresponding to a carrier density of about 10^{11} cm^{-2}.

Figure 1(a) shows normalized pump-probe traces at different positions across the FIB pattern of sample *A*. The overall shape and the initial decay strongly depend on the position. To quantify this position dependence, we have fitted the experimental traces to double-exponential functions $A \exp(-\Delta t/\tau_1) + B \exp(-\Delta t/\tau_2)$ where Δt is the time delay
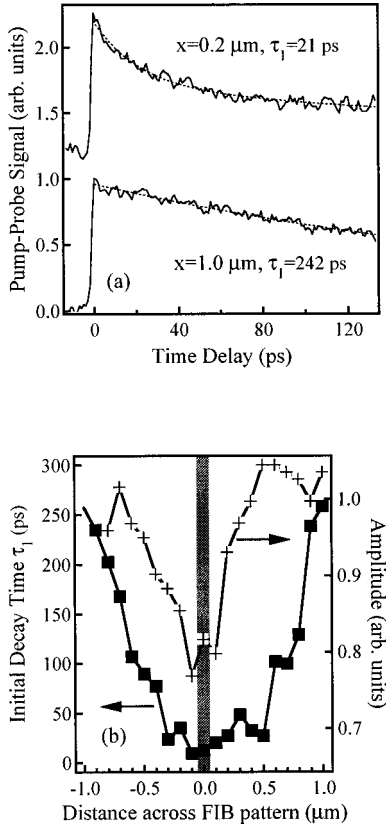
FIG. 1. Sample *A* (100-nm implanted stripes, 2000-nm spaces): (a) Normalized pump-probe traces at different distances *x* away from the stripes, experimental traces (solid), double exponential fits (dotted) from which the initial decay time τ_1 is obtained. (b) Initial decay time τ_1 (squares) and pump-probe amplitude at zero time delay (crosses) vs. position. The gray bar marks the implanted stripe.

between pump and probe pulse. Here, τ_1 is the faster time constant and describes the initial decay while τ_2 is the slower time constant, which describes the decay at longer times. A detailed discussion of the physical meaning of τ_1 and τ_2 will be presented later. From our data, we find that τ_2 is 200–300 ps, independent of the spatial position.

The faster initial decay time τ_1 and the pump-probe amplitude at $\Delta t = 0$ are plotted versus position in Fig. 1(b). The amplitude is reduced in the implanted stripe, as expected.[15,16] Midway between the implanted stripes, the decay time τ_1 is roughly equal to 250 ps. Surprisingly, the decay times over an 800-nm-wide range around the 100-nm implanted stripe are much shorter at about 10–40 ps. Note that the pump-probe traces decay almost exponentially with a time constant of roughly 250 ps far away from the FIB patterned area. This decay time is independent of position and will be referred to as recombination time in the following.[17] The short decay times around the implanted stripe cannot be due to recombination. Furthermore, they cannot be caused by spatial averaging with the fast trapping times in the implanted stripes since the rise in the amplitude signal shows that spatial averaging effects happen on a much shorter spatial scale. Finally, carrier trapping due to a wider damage profile cannot be the reason for these short decay times either since the large amplitude, i.e., large nonlinearity, in much of this region shows that the implantation-induced defect distribution

is not much broader than the nominal stripe width of 100 nm, as expected from the TRIM simulations.[13]

We conclude that the short decay times τ_1 of 10–40 ps result from carrier transport. In general, both carrier diffusion and drift can contribute to the transport. Carrier drift requires potential gradients. We note that the sample does not contain potential gradients in the plane of the quantum well before implantation. Moreover, the implantation is not expected to result in large potential gradients. This is because ion implantation into GaAs generates As antisites.[18] These defect states are located close to the center of the band gap[19] and pin the Fermi level at midgap.[20] Since the Fermi level in the unimplanted regions is also at midgap in the undoped quantum well, we do not expect the formation of large potential gradients. Moreover, we do not expect the formation of large potential gradients due to compositional intermixing, which gives large energy shifts only at ion doses higher than the ones used in our samples.[21] Consequently, we conclude that carrier drift can be neglected and that carrier transport is mainly due to diffusion of carriers towards the implanted stripe. Diffusion is driven by the carrier density gradient that is caused by the fast trapping of carriers in the stripe. This conclusion is confirmed by quantitative modeling which includes diffusion but neglects drift. Since the optical excitation of excitons is followed by ionization after about 300 fs at room temperature,[22] the dynamics of the density *n* of band electron-hole pairs is modeled. We have solved the one-dimensional continuity equation for the electron-hole pair density *n*, coupled to the differential equation for the density n_t of occupied traps

$$\frac{\partial n(x,t)}{\partial t} = D_a \frac{\partial^2 n}{\partial x^2} - \frac{n}{\tau_{rec}} - \frac{n}{\tau_t(x)} \left(1 - \frac{n_t}{N_0} \right) + G(t), \quad (1)$$

$$\frac{\partial n_t(x,t)}{\partial t} = \frac{n}{\tau_t(x)} \left(1 - \frac{n_t}{N_0} \right). \quad (2)$$

Here, D_a is the ambipolar diffusion constant,[23,24] τ_{rec} is the recombination time, τ_t is the trapping time, and N_0 is the total density of traps in the implanted stripes. The spatially uniform carrier excitation is described by the *x*-independent generation term $G(t)$, for which we assume a $sech^2$ pulse with a full width at half maximum of 200 fs. The trapping rate $1/\tau_t$ decreases from a constant value in the implanted stripes to zero outside the stripes. This decrease occurs over a 20-nm-wide transition region, determined from the TRIM simulations. Trap filling and the corresponding decrease of the trapping rate with time are accounted for in the third term on the RHS of Eq. (1) in conjunction with Eq. (2). The degree of trap filling is adjusted by the ratio $N_0 / \int G(t)dt$ in the implanted stripes.

The initial exciton ionization[22] as well as the thermalization of carriers with the lattice are not included in the model. At room temperature, the latter occurs in about a picosecond if carriers are injected at the band edge of $GaAs/Al_xGa_{1-x}As$ quantum wells.[25,26] Therefore, Eqs. (1) and (2) are used for time delays of 2 ps and longer. Moreover, for these time delays, the ambipolar diffusion constant D_a for room temperature can be used, neglecting any temperature dependence of diffusion.[24]
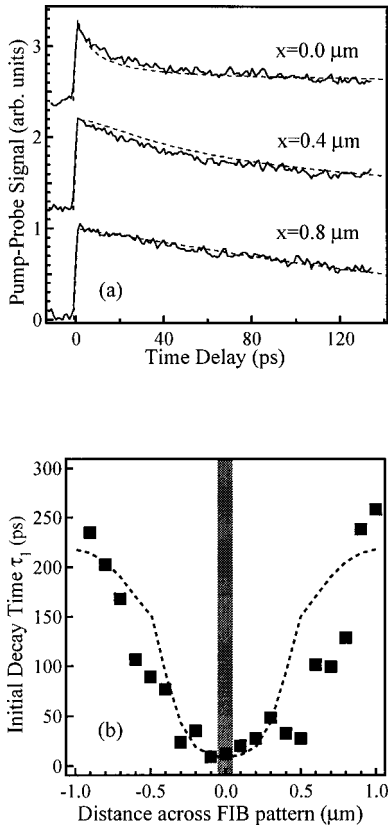
FIG. 2. Sample *A*: (a) Measured (solid) and calculated (dashed) pump-probe traces at different positions, see text for the details of the calculation. (b) Initial decay times from double exponential fits to measured (squares) and calculated (dashed line) pump-probe traces vs. position.
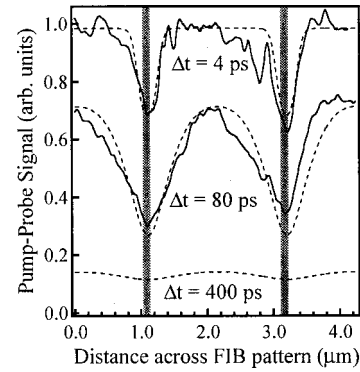

FIG. 3. Sample *A*: Measured (solid) and calculated (dashed) pump-probe signal vs. position for different time delays. Averaging over a 300-nm tip aperture was assumed in the calculation.

In order to compare the calculated electron-hole pair density n to the measured pump-probe traces, we assume that the pump-probe signal is proportional to n.[27] Figure 2(a) shows measured and calculated pump-probe traces at different positions across the FIB pattern. For all positions, the calculation was performed with $D_a = 10$ cm^2/s, $\tau_{rec} = 250$ ps, $\tau_t = 3$ ps, and $N_0 / \int G(t) dt = 4$ to account for trap filling. The value for D_a is reasonable in view of earlier work on GaAs/Al$_x$Ga$_{1-x}$As heterostructures and quantum wells.[23,24] The good agreement between the experimental and the calculated pump-probe traces proves that diffusion substantially affects the dynamics in sample *A* and strongly supports the argument that carrier drift can be neglected. Fig. 2(b) shows the faster time constants τ_1, from double exponential fits to the measured and calculated pump-probe traces, versus position. Again, good agreement is obtained.

More details of the diffusion dynamics can be inferred from direct measurements of the pump-probe signal versus distance across the FIB pattern for fixed time delays Δt. These data are shown in Fig. 3. At an early time delay, $\Delta t = 4$ ps, we observe a squarelike pump-probe distance dependence, corresponding to a square-like carrier density profile. At a later time delay, $\Delta t = 80$ ps, a smoother, quasisinusoidal profile is observed. These measurements show a good fit to the calculated profiles, which use the parameters obtained from the modeling in Fig. 2. The calculated carrier profile at $\Delta t = 400$ ps is also shown,[28] revealing a profile which is al-

most flat. We conclude that the initial squarelike profile at $\Delta t = 4$ ps is a result of the fast carrier trapping in the well-defined FIB implanted stripes. Enhanced diffusion at the edges of the squarelike carrier profile then smoothes out the sharp edges, leading to the quasisinusoidal profile at $\Delta t = 80$ ps. At $\Delta t = 400$ ps, the flat carrier profile shows that diffusion has evened out the carrier density gradients.

The smoothing of the initial squarelike carrier profile in Fig. 3 results in the spatially dependent decay time τ_1 shown in Fig. 2. Fast decay times are observed close to the edges due to strong diffusion. In contrast, midway between the implanted stripes, diffusion is slow and the decay time τ_1 is much longer.

These effects can also be understood in the spatial frequency domain. We recall that, in a sinusoidal carrier distribution with period L, the carrier density exponentially decays due to diffusion with a time constant $\tau_D = L^2 / (4\pi^2 D_a)$.[29] The linearity of the continuity equation implies that the dynamics of a *nonsinusoidal* periodic profile is simply the sum of the dynamics of its harmonic components. These arguments show that the higher spatial harmonics of the initial squarelike carrier profile decay much faster than the fundamental period due to their smaller L. The fast decay of higher spatial harmonics corresponds to the smoothing of the edges of the carrier profile in real space. Since the higher spatial harmonics decay much faster than the fundamental period, a quasisinusoidal profile is expected at long times, as observed in Fig. 3. With respect to the position dependence of the diffusion decay time $\tau_D = L^2 / (4\pi^2 D_a)$, we note that this decay time does not depend on position in sinusoidal carrier distributions.[29] Summarizing this discussion, we can distinguish two different diffusion regimes: (i) An initial diffusion regime, which is characterized by a squarelike carrier profile containing higher spatial harmonics, and by position-dependent temporal diffusion decay, and (ii) a long-time diffusion regime, in which the carrier profile is quasisinusoidal with only weakly position-dependent temporal diffusion decay.

We now comment on the physical meaning of the time constants τ_1 and τ_2 of the double-exponential fit. The time constant τ_1 describes the initial diffusion regime. Close to the edges of the implanted stripes, τ_1 is much faster than the recombination time due to the fast diffusion corresponding to the decay of the higher spatial harmonics in the initial diffu-
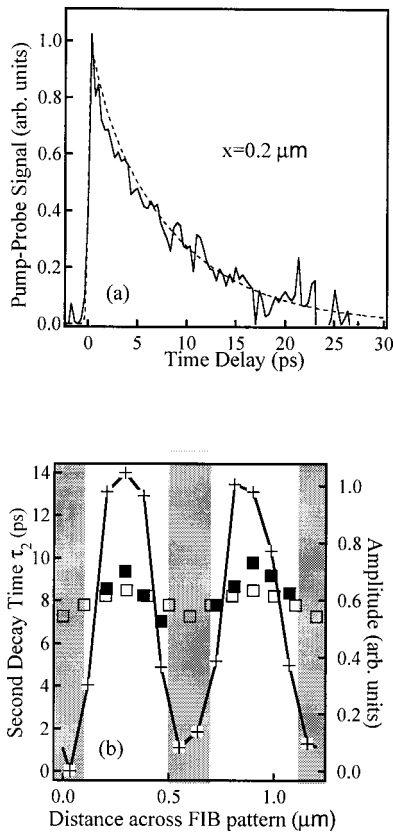
FIG. 4. Sample *B* (200-nm implanted stripes, 400-nm spaces): (a) Measured (solid) and calculated (dashed) normalized pump-probe trace 0.2 μm away from the center of an implanted stripe. (b) Second decay time, describing the long-time diffusion regime in sample *B*, from fits to measured (filled squares) and calculated (open squares) pump-probe traces and pump-probe amplitude at zero time delay (crosses) vs. position.

sion regime. Midway between the stripes, the diffusion current is negligible in the initial diffusion regime since the carrier profile is almost flat with negligible gradient. Therefore, τ_1 reflects the recombination time midway between the implanted stripes in sample *A*. In fact, the time constant $\tau_1 = 250$ ps determined experimentally midway between the stripes is identical to the recombination time determined far away from the FIB patterned area.

In the long-time diffusion regime, diffusion with $D_a = 10$ cm^2/s in a sinusoidal profile with period $L = 2.1$ μm leads to a decay of the carrier density with the time constant $\tau_D = 110$ ps in sample *A*. This number is relatively close to the recombination time $\tau_{rec} = 250$ ps. Therefore, both recombination and diffusion contribute to the decay of the pump-probe traces from sample *A* at long times. This long-time decay is described by the slow time constant τ_2. We have

found that τ_2 is 200–300 ps from fits to both experimental and calculated pump-probe traces, in agreement with the combined recombination and diffusion dynamics. This discussion shows, that sample *A* is not appropriate for the experimental observation of the long-time diffusion regime unperturbed by recombination.

The long-time diffusion regime is experimentally more accessible in sample *B* (200-nm implanted stripes, 400-nm spaces) in which the overall diffusion is much faster due to the smaller distances. Figure 4(a) shows a measured and a calculated pump-probe trace. The calculation uses $D_a = 20$ cm^2/s, $\tau_{rec} = 100$ ps (Ref. 17) measured far away from the FIB patterned area, and $\tau_t = 0.3$ ps. The faster trapping time as compared to sample *A* reflects the higher implantation dose. Trap filling could be neglected in sample *B* due to the larger dose and the larger ratio of implanted to unimplanted area.

Both the experimental and the calculated pump-probe traces show a single exponential decay in the time window from 2 to 30 ps. This is because the higher spatial harmonics have diffusion decay times of less than 2 ps in sample *B* and the initial diffusion regime is already over at 2 ps. This implies that the term $A \exp(-\Delta t/\tau_1)$ of the fit function $A \exp(-\Delta t/\tau_1) + B \exp(-\Delta t/\tau_2)$ has decayed to zero in the time window of observation. Therefore, a single exponential decay is obtained and τ_2 can be determined from a fit to function $B \exp(-\Delta t/\tau_2)$.

The decay times τ_2 of measured and calculated traces are plotted versus position in Fig. 4(b) together with the pump-probe amplitude at $\Delta t = 0$. Between the implanted stripes, the time constants τ_2 of about 8 ps are much faster than the recombination time. Spatial averaging and trapping do not determine these time constants, as shown by the rise of the amplitude and the arguments presented for sample *A*. The decay between the implanted stripes is dominated by diffusion in the long-time diffusion regime, unperturbed by the much slower recombination. The decay time depends only very weakly on position, as expected for quasisinusoidal carrier profiles in this regime. We note that diffusion could not have been studied by far-field transient grating techniques[30] in sample *B* since diffraction of 800-nm light from a grating with a 600-nm period is impossible.

In conclusion, femtosecond near-field spectroscopy has allowed us to experimentally observe different diffusion regimes in semiconductor nanostructures. The results directly demonstrate a complex dependence of spatiotemporal carrier dynamics on the lateral structure and the time window of observation.

*FAX: +41-1-6331059. Electronic address:
 acherman@iqe.phys.ethz.ch
†Present address: Micrion GmbH, D-85622 Feldkirchen, Germany.

[1] A. Richter, G. Brehme, M. Süptitz, C. Lienau, T. Elsässer, M. Ramsteiner, R. Nötzel, and K. H. Ploog, Phys. Rev. Lett. **79**, 2145 (1997).
[2] A. Richter, M. Süptitz, D. Heinrich, C. Lienau, T. Elsässer, M. Ramsteiner, R. Nötzel, and K. H. Ploog, Appl. Phys. Lett. **73**, 2176 (1998).
[3] J. Levy, V. Nikitin, J. M. Kikkawa, A. Cohen, N. Samarth, R. Garcia, and D. D. Awschalom, Phys. Rev. Lett. **76**, 1948 (1996).
[4] R. D. Grober, T. D. Harris, J. K. Trautman, E. Betzig, W. Wegscheider, L. Pfeiffer, and K. West, Appl. Phys. Lett. **64**, 1421 (1994).

[5] Y. Toda, M. Kourogi, M. Ohtsu, Y. Nagamune, and Y. Arakawa, Appl. Phys. Lett. **69**, 827 (1996).

[6] A. Hartmann, Y. Ducommun, L. Loubies, K. Leifer, and E. Kapon, Appl. Phys. Lett. **73**, 2322 (1998).

[7] M. Yoshita, M. Baba, S. Koshiba, H. Sakaki, and H. Akiyama, Appl. Phys. Lett. **73**, 2965 (1998).

[8] S. Haacke, M. Hartig, D. Y. Oberli, B. Deveaud, E. Kapon, U. Marti, and F. K. Reinhart, Solid-State Electron. **40**, 299 (1996).

[9] J. B. Stark, U. Mohideen, and R. E. Slusher, in *Quantum Electronics Conference*, Vol. 16 of OSA Tech. Dig. Ser. (OSA, Washington, D.C., 1995), p. 82.

[10] A. Vertikov, M. Kuball, A. V. Nurmikko, and H. J. Maris, Appl. Phys. Lett. **69**, 2465 (1996).

[11] S. Smith, N. C. R. Holme, B. Orr, R. Kopelman, and T. Norris, Ultramicroscopy **71**, 213 (1998).

[12] B. A. Nechay, U. Siegner, F. Morier-Genoud, A. Schertel, and U. Keller, Appl. Phys. Lett. **74**, 61 (1999).

[13] J. F. Ziegler, J. P. Biersack, and U. Littmark, *The Stopping and Range of Ions in Solids* (Pergamon, New York, 1989), Vol. 1.

[14] M. Lambsdorff, J. Kuhl, J. Rosenzweig, A. Axmann, and J. Schneider, Appl. Phys. Lett. **58**, 1881 (1991).

[15] M. J. Lederer, B. Luther-Davies, H. H. Tan, C. Jagadish, M. Haiml, U. Siegner, and U. Keller, Appl. Phys. Lett. **74**, 1993 (1999).

[16] Y. Silverberg, P. W. Smith, D. A. B. Miller, B. Tell, A. C. Gossard, and W. Wiegmann, Appl. Phys. Lett. **46**, 701 (1985).

[17] The recombination times in samples *A* and *B* are not due to intrinsic radiative recombination but result from nonradiative decay due to a small laterally uniform background implantation dose applied in the FIB patterning process. The background implantation dose varies between FIB implantation runs. This results in different recombination times in samples *A* and *B*.

[18] W. Walukiewicz, Z. Liliental-Weber, J. Jasinski, M. Almonte, A. Prasad, E. E. Haller, E. R. Weber, P. Grenier, and J. F. Whitaker, Appl. Phys. Lett. **69**, 2569 (1996).

[19] P. Omling, P. Silverberg, and L. Samuelson, Phys. Rev. B **38**, 3606 (1988).

[20] G. L. Witt, Mater. Sci. Eng., B **22**, 9 (1993).

[21] P. G. Piva, P. J. Poole, M. Buchanan, G. Champion, I. Templeton, G. C. Aers, R. Williams, Z. R. Wasilewski, E. S. Koteles, and S. Charbonneau, Appl. Phys. Lett. **65**, 621 (1994).

[22] W. H. Knox, R. L. Fork, M. C. Downer, D. A. B. Miller, D. S. Chemla, C. V. Shank, A. C. Gossard, and W. Wiegmann, Phys. Rev. Lett. **54**, 1306 (1985).

[23] A. Olsson, D. J. Erskine, Z. Y. Xu, A. Schremer, and C. L. Tang, Appl. Phys. Lett. **41**, 659 (1982).

[24] H. Hillmer, A. Forchel, and C. W. Tu, Phys. Rev. B **45**, 1240 (1992).

[25] Y. L. Lam and J. Singh, IEEE J. Quantum Electron. **31**, 923 (1995).

[26] A. M. T. Kim, S. Hunsche, T. Dekorsy, H. Kurz, and K. Köhler, Appl. Phys. Lett. **68**, 2956 (1996).

[27] J. Shah, *Ultrafast Spectroscopy of Semiconductors and Semiconductor Nanostructures* (Springer-Verlag, Berlin, 1996).

[28] For very long time delays, the measured pump-probe signal is so small that noise prevents detailed analysis. Therefore, only the calculated trace is shown in Fig. 3.

[29] H. J. Eichler, P. Guenter, and D. W. Pohl, *Laser-Induced Dynamic Gratings* (Springer-Verlag, Berlin, 1986).

[30] T. Chang, H. Kim, and H. Yu, Chem. Phys. Lett. **111**, 64 (1984).